View metadata, citation and similar papers at core.ac.uk

brought to you by CORE

provided by Sound Ideas

University of Puget Sound
Sound Ideas

All Faculty Scholarship | Faculty Scholarship

2013

Neutrino tomography

David C. Latimer
University of Puget Sound, dlatimer@pugetsound.edu

Margaret A. Millhouse
University of Puget Sound

Follow this and additional works at: http://soundideas.pugetsound.edu/faculty_pubs

Citation
Millhouse, Margaret A, and David C. Latimer. "Neutrino Tomography." American Journal of Physics. 81.9 (2013): 646. Print.

This Article is brought to you for free and open access by the Faculty Scholarship at Sound Ideas. It has been accepted for inclusion in All Faculty Scholarship by an authorized administrator of Sound Ideas. For more information, please contact soundideas@pugetsound.edu.

AAPT PHYSICS EDUCATION | AMERICAN JOURNAL of PHYSICS

Neutrino tomography

Margaret A. Millhouse and David C. Latimer

Citation: American Journal of Physics **81**, 646 (2013); doi: 10.1119/1.4817314
View online: http://dx.doi.org/10.1119/1.4817314
View Table of Contents: http://scitation.aip.org/content/aapt/journal/ajp/81/9?ver=pdfcov
Published by the American Association of Physics Teachers

Articles you may be interested in

Expectations for neutron-antineutron oscillation time from TeV scale baryogenesis
AIP Conf. Proc. **1534**, 211 (2013); 10.1063/1.4807359

Constraint on slepton intergenerational mixing from big-bang nucleosynthesis
AIP Conf. Proc. **1467**, 286 (2012); 10.1063/1.4742119

Flavor group Δ (3 n 2)
J. Math. Phys. **48**, 073501 (2007); 10.1063/1.2734865

Tau-Mu Flavor Violation and the Scale of New Physics
AIP Conf. Proc. **698**, 478 (2004); 10.1063/1.1664282

Neutrino Theories
AIP Conf. Proc. **540**, 75 (2000); 10.1063/1.1328880

This article is copyrighted as indicated in the article. Reuse of AAPT content is subject to the terms at: http://scitation.aip.org/termsconditions. Downloaded to IP: 207.207.127.233 On: Wed, 06 May 2015 16:28:56

Neutrino tomography

Margaret A. Millhouse and David C. Latimer
Department of Physics, Reed College, Portland, Oregon 97202

(Received 2 July 2012; accepted 17 July 2013)

Neutrinos are produced in weak interactions as states with definite flavor—electron, muon, or tau—and these flavor states are superpositions of states of different mass. As a neutrino propagates through space, the different mass eigenstates interfere, resulting in time-dependent flavor oscillation. Though matter is transparent to neutrinos, the flavor oscillation probability is modified when neutrinos travel through matter. Herein, we present an introduction to neutrino propagation through matter in a manner accessible to advanced undergraduate students. As an interesting application, we consider neutrino propagation through matter with a piecewise-constant density profile. This scenario has relevance in neutrino tomography, in which the density profile of matter, like the Earth's interior, can be probed via a broad-spectrum neutrino beam. We provide an idealized example to demonstrate the principle of neutrino tomography. © *2013 American Association of Physics Teachers.*
[http://dx.doi.org/10.1119/1.4817314]

I. INTRODUCTION

In the standard model of particle physics, the neutrino comes in three flavors, each paired with one of the charged leptons. Neutrinos were originally assumed to be massless, but the first hint that this was not the case came from solar neutrino experiments. The standard solar model (SSM)[1] predicts the expected flux of neutrinos incident upon the Earth; however, experimental detection of solar neutrinos indicated a flux that ranged from 30% to 60% of the expected values.[2–5] These experiments primarily detected electron neutrinos. The Sudbury Neutrino Observatory employed elements in its neutrino detector that were sensitive to all flavors. By its count, the total neutrino flux was consistent with the expectations from the SSM.[6] Presently, the overwhelming majority of experiments that detect neutrinos from disparate sources—atmospheric,[7] reactor,[8,9] and accelerator beam-stop neutrinos[10,11]—can be understood in terms of three massive neutrinos that mix nontrivially.[12]

A historical overview of neutrino physics can be found in this journal,[13] including an overview of the experiments that have led to our current understanding of oscillations.[14,15] In order for neutrinos to undergo flavor oscillation, two conditions must be met. First, the neutrinos must be massive; second, the flavor states, created through the weak interactions, must be superpositions of these mass eigenstates.

Neutrinos travel at highly relativistic speeds, yet neutrino oscillations can be understood using tools from a first course in quantum mechanics. Indeed, one introductory quantum mechanics text discusses two-flavor neutrino oscillations as an example of a two-state system.[16] In Sec. II, we derive the neutrino oscillation formula for three neutrinos propagating in vacuum. In light of the known values of the neutrino oscillation parameters, we discuss how a given neutrino experiment can be understood within the framework of only two oscillating neutrinos.

Though neutrino propagation through vacuum conveys the essential physics of flavor oscillations, a key component in understanding solar and atmospheric neutrino data is the impact that dense media have upon the neutrino oscillations. Dense media like the Sun's or Earth's interior are largely transparent to neutrinos; however, the neutrino oscillation parameters are modified via an effective index of refraction, a consequence of the coherent forward scattering of the neutrinos by the background matter. In Sec. III, we derive the oscillation formula for a two-flavor system of neutrinos that travel through matter of constant density and demonstrate the impact that matter plays upon neutrinos traveling through the Earth's mantle and core. The derivation relies upon the generalized index of refraction formula in dilute media.[17] This formula is an interesting application of scattering theory appropriate for the second semester of an undergraduate quantum mechanics course, and we reproduce its derivation in the Appendix.

An understanding of neutrino-matter interactions opens up a rich new class of examples that can be explored by undergraduates. As a simple application, we derive in Sec. IV, the oscillation probability for neutrinos traveling through matter with a piecewise-constant density profile. This matter profile has significance because atmospheric neutrinos that traverse the entire diameter of the Earth encounter a density that can be approximated as piecewise-constant; that is, the Earth can be modeled as a dense core surrounded by a less-dense mantle.[18] Through a series of examples we show how the size and location of an inhomogeneity in an otherwise constant-density matter profile affects the neutrino oscillation probability.

Though the neutrino itself is still an object of intense study, as our knowledge of the neutrino oscillation parameters becomes more precise, the neutrino can become a tool to study other physical systems. In particular, since neutrinos interact very weakly with matter, solar neutrinos can stream through the Sun virtually unaltered, carrying with them information about the nuclear processes that produced them. As another application, one can use a beam of neutrinos to probe the density profile of the interior of an object like the Earth; this is the goal of neutrino tomography. From the detected neutrinos, one can gain clues about the electron density of the material through which they travel. Accessible overviews of neutrino tomography can be found in Refs. 19 and 20, and in Sec. V, we provide an explicit demonstration of these ideas in an idealized simulation. Assuming an ideal broadband neutrino source and detector, we show how the analysis of the neutrino oscillation probability at the detector can be used to identify the position of an inhomogeneity in an otherwise constant-density region of the Earth.

II. VACUUM OSCILLATION

Neutrino oscillation data are consistent with the existence of three neutrino eigenstates ν_j of distinct mass m_j, $j = 1, 2, 3$.

This article is copyrighted as indicated in the article. Reuse of AAPT content is subject to the terms at: http://scitation.aip.org/termsconditions. Downloaded to IP: 207.207.127.233 On: Wed, 06 May 2015 16:28:56

Representing one of these weak interaction states as ν_α, where $\alpha = e, \mu, \tau$, we relate the flavor states to the mass eigenstates through a unitary 3×3 mixing matrix U:

$$\nu_\alpha = \sum_{j=1}^{3} U_{\alpha j} \nu_j. \tag{1}$$

A general 3×3 unitary matrix can be parameterized with nine real parameters; however, several of these parameters cannot be probed with neutrino oscillations. For neutrino oscillations, the Pontecorvo-Maki-Nakagawa-Sakata (PMNS) mixing matrix[21,22] can be parameterized with four real parameters, consisting of three mixing angles θ_{jk} and a phase δ:

$$U = \begin{pmatrix} 1 & 0 & 0 \\ 0 & \cos\theta_{23} & \sin\theta_{23} \\ 0 & -\sin\theta_{23} & \cos\theta_{23} \end{pmatrix} \times \begin{pmatrix} \cos\theta_{13} & 0 & e^{i\delta}\sin\theta_{13} \\ 0 & 1 & 0 \\ -e^{-i\delta}\sin\theta_{13} & 0 & \cos\theta_{13} \end{pmatrix} \times \begin{pmatrix} \cos\theta_{12} & \sin\theta_{12} & 0 \\ -\sin\theta_{12} & \cos\theta_{12} & 0 \\ 0 & 0 & 1 \end{pmatrix}. \tag{2}$$

Aside from the phase, the PMNS matrix is a product of three two-dimensional rotations of a plane. A global analysis of the neutrino experimental data is consistent with the mixing angles $\theta_{12} = 34^\circ \pm 1^\circ$, $\theta_{13} = 8.9^\circ \pm 0.5^\circ$, and $\theta_{23} = 39^\circ \pm 2^\circ$; the value of the phase δ is poorly constrained.[23]

The evolution of this system is governed by the states of definite mass. Supposing that the neutrino has definite momentum p, for each mass eigenstate, we have

$$i\partial_t \nu_j(t) = E_j \nu_j(t), \quad \text{with} \quad E_j = \sqrt{m_j^2 + p^2}, \tag{3}$$

where we choose a system of units in which $\hbar = c = 1$. Cosmological bounds place neutrino rest masses on the scale of electronvolts.[24] Typical neutrino energies are at least on the MeV scale, so we make the relativistic approximation

$$E_j \simeq p\left(1 + \frac{m_j^2}{2p^2}\right) \simeq p + \frac{m_j^2}{2E}, \tag{4}$$

where the final energy E neglects the size of m_j at this order of approximation. From this, we can determine the time evolution of the weak interaction states, which we represent as a column vector $\nu(t) = (\nu_e(t), \nu_\mu(t), \nu_\tau(t))^T$:

$$i\partial_t \nu(t) = \left[\left(p + \frac{m_1^2}{2E}\right)\mathbb{I} + \frac{1}{2E} U\,\mathrm{diag}(0, \Delta_{21}, \Delta_{31})\, U^\dagger\right]\nu(t), \tag{5}$$

where $\mathbb{I}$ is the 3×3 identity matrix and $\Delta_{jk} = m_j^2 - m_k^2$ are the mass-squared differences. Expressing the exponential of a matrix through its power series, the solution to this differential equation is simply

$$\nu(t) = \exp[-iH_0 t]\nu(0). \tag{6}$$

In the exponential, we drop the part of the vacuum Hamiltonian proportional to the identity and define

$$H_0 = \frac{1}{2E} U\,\mathrm{diag}(0, \Delta_{21}, \Delta_{31})\, U^\dagger. \tag{7}$$

As any multiple of the identity commutes with H_0, upon exponentiation, the identity term will result in an unmeasurable overall phase on the state $\nu(t)$, which we omit for the sake of convenience.

With the time evolution of the system established, we can determine the neutrino oscillation probability. Suppose a localized source emits neutrinos of flavor α at time $t = 0$, i.e., $\nu(0) = \nu_\alpha$. Then some time t after leaving the source, the probability of detecting neutrinos of flavor β in the beam is

$$\mathcal{P}_{\alpha\to\beta}(t) = |\langle \nu_\beta | \nu(t) \rangle|^2. \tag{8}$$

Typically, the neutrino source and detector occupy fixed positions, and it is much more convenient to speak of their separation baseline L. As the neutrinos are ultrarelativistic, one has $t \simeq L$ (where $c = 1$) so we can express the oscillation probability as

$$\mathcal{P}_{\alpha\to\beta}(L) = \delta_{\alpha\beta} - 4 \sum_{\substack{k<j \\ j,k=1}}^{3} (U_{\alpha j} U_{\alpha k} U_{\beta k} U_{\beta j}) \sin^2\left(\frac{\Delta_{jk} L}{4E}\right), \tag{9}$$

where, for simplicity, we have chosen the phase $\delta = 0$. We note the appearance of four factors of the PMNS matrix elements in the formula. This is because the evolution of a flavor state involves a rotation to the mass basis, evolution of the mass state, and then a rotation back to the flavor basis, resulting in two factors of PMNS matrix elements. A careful examination of this equation demonstrates the two requirements for neutrino oscillation: at least two of the massive eigenstates must have distinct masses and mix nontrivially.

For a neutrino beam with a narrow energy spectrum, there are ostensibly three length scales over which neutrino oscillations occur. For each mass-squared difference, we can characterize these length scales with the vacuum oscillation wavelength $\lambda_0 = 4\pi E/\Delta_{jk}$. In fact, the measured values of the mass-squared differences are[23] $\Delta_{21} = 7.5^{+0.3}_{-0.2} \times 10^{-5}$ eV^2 and $|\Delta_{32}| = 2.4^{+0.1}_{-0.1} \times 10^{-3}$ eV^2. Since these two mass-squared differences are on vastly different scales and $\Delta_{31} = \Delta_{32} + \Delta_{21}$, oscillations actually occur over two rather distinct length scales: those driven by Δ_{21} and those driven by $\Delta_{31} \approx \Delta_{32}$. Coupling this with the smallness of the mixing angle θ_{13}, one can interpret, to a good approximation, an individual neutrino experiment as the oscillation between two neutrino states. The figure of merit needed to determine the relevant oscillation scale in an experiment is the range of the values of the ratio L/E that the experiment spans. For instance, if the baseline-to-energy ratio for an experiment satisfies $\Delta_{21} L/E \sim \mathcal{O}(1)$, then the oscillatory terms in Eq. (9) for the other two mass-squared differences will not be resolvable by a detector. In this case, we can average over these oscillations, resulting in

$$\left\langle \sin^2\left(\frac{\Delta_{32} L}{4E}\right)\right\rangle_{\text{avg}} = \left\langle \sin^2\left(\frac{\Delta_{31} L}{4E}\right)\right\rangle_{\text{avg}} = \frac{1}{2}. \tag{10}$$

This article is copyrighted as indicated in the article. Reuse of AAPT content is subject to the terms at: http://scitation.aip.org/termsconditions. Downloaded to IP: 207.207.127.233 On: Wed, 06 May 2015 16:28:56

One oscillating term remains in the probability, Eq. (9), and if we make the approximation $\theta_{13} = 0$, then the electron neutrino survival probability is

$$\mathcal{P}_{e\to e} \simeq 1 - \sin^2 2\theta_{12} \sin^2\left(\frac{\Delta_{12}L}{4E}\right). \tag{11}$$

This is identical to the survival probability for two flavors. In the appearance channel, electron neutrinos oscillate into roughly an equal admixture of muon and tau neutrinos, which we will refer to simply as ν_α. As this process is unitary, the appearance oscillation probability is then

$$\mathcal{P}_{e\to\alpha} \simeq \sin^2 2\theta_{12} \sin^2\left(\frac{\Delta_{12}L}{4E}\right). \tag{12}$$

In what follows, we shall only consider a two-neutrino system, consisting of ν_e and ν_α. This greatly simplifies the formulae without trivializing the physics. This approximation will be valid so long as we consider baseline and neutrino energies that satisfy $L/E \sim \Delta_{21}^{-1} \sim 10^4$ m/MeV. If we consider reactor neutrinos as our source, their energy range is from 1 to 10 MeV so that the relevant baselines are on the order of kilometers. As there is only one mixing angle and mass-squared difference, we will drop the subscripts to ease the notation and set $\theta = \theta_{12}$ and $\Delta = \Delta_{21}$. For this two-neutrino system, the mixing matrix can be parameterized by the single mixing angle θ; it takes the familiar form of a rotation matrix in the plane:

$$\begin{pmatrix}\nu_e\\ \nu_\alpha\end{pmatrix} = \begin{pmatrix}\cos\theta & \sin\theta\\ -\sin\theta & \cos\theta\end{pmatrix}\begin{pmatrix}\nu_1\\ \nu_2\end{pmatrix}. \tag{13}$$

Strictly speaking, the state ν_2 in the above equation actually represents a linear combination of mass eigenstates ν_2 and ν_3; however, the point remains that in this restricted region of parameter space a two-neutrino subspace decouples from the full three-neutrino picture.

III. MATTER INTERACTIONS

Vacuum oscillations alone are not sufficient to account for all neutrino data; see Ref. 12 for a review. Neutrinos' interactions with the matter through which they travel are crucial in accommodating the solar and atmospheric neutrino data. Though neutrinos interact very weakly, their propagation is modified in a manner akin to that experienced by light traveling through a transparent medium. The index of refraction for light through a dilute medium can be related to microscopic properties of the medium by computing the interference between the largely transmitted incident beam and the scattered waves.[25,26] For a random distribution of scatterers, only the forward portion of the scattered waves will interfere constructively; as a result, the deviation of the refractive index from unity is proportional to the forward scattering amplitude and the density of scatterers.

The analysis was extended to particle physics by Fermi.[17] His derivation is an interesting application of nonrelativistic scattering theory, appropriate for undergraduate students; we have reproduced the arguments in the Appendix. As with light, the index of refraction for a particle of momentum p in a dilute medium of scatterers with number density N is related to the forward scattering amplitude $f(0)$ according to

$$n = 1 + 2\pi N\frac{f(0)}{p^2}. \tag{14}$$

Neutrinos are ultrarelativistic and travel through dense media, but it has been shown that this equation holds regardless.[27] The index of refraction modifies the momentum of the particle in the medium, $\tilde{p} = np$, which can be regarded as adding effective mass to the particle:

$$E^2 = \tilde{p}^2 + m^2 \approx p^2 + 4\pi N f(0) + m^2, \tag{15}$$

neglecting the term that is proportional to $(n-1)^2$. This extra term in the dispersion relation can be accounted for by adding a small effective potential, $V = 2\pi N f(0)/E$, to the Hamiltonian. Both Mikheyev and Smirnov[28] and Wolfenstein[29] independently described this MSW effect for neutrinos propagating through matter.

To compute the forward scattering amplitude for neutrinos in matter, we recall that neutrinos interact via the weak force, a short-range force mediated by either the neutral Z^0 boson or the charged $W^\pm$ boson.[30] Through the neutral current, all three neutrino flavors interact with ordinary matter (comprised of electrons and up and down quarks) with equal strength. As a result, the neutral-current contribution to the forward scattering amplitude is the same for all flavors. Adding this interaction to the Hamiltonian H_0 will result in a potential that is proportional to the identity. As before, such terms result in an unmeasurable phase and do not affect the oscillation probability. On the other hand, charged-current interactions are flavor dependent. The W boson couples electrons with electron neutrinos, and it also couples up and down quarks. For instance, an incoming electron neutrino can exchange a W boson with a down quark in a neutron resulting in a proton and electron, $\nu_e + n \to e^- + p$. As we are interested only in coherent forward scattering, this process is irrelevant. The only relevant process is $\nu_e + e^- \to \nu_e + e^-$, mediated by the charged weak interaction, Fig. 1. Keeping only the leading-order term, the charged-current contribution to the forward scattering amplitude is $f(0) = G_F E/\sqrt{2}\pi$, where G_F is Fermi's constant. Thus, neglecting neutral-current interactions, we add to the Hamiltonian a potential $V = \sqrt{2}G_F N_e$ for the electron flavor *only*, with N_e the local electron density. For electron antineutrinos, the potential acquires a minus sign.

Within the two-neutrino framework, neutrino evolution in matter is governed by a new Hamiltonian $H_m(x)$:

$$i\partial_t\begin{pmatrix}\nu_e(t)\\ \nu_\alpha(t)\end{pmatrix} = \frac{1}{4E}\begin{pmatrix}-\cos 2\theta\Delta + 4EV(x) & \sin 2\theta\Delta\\ \sin 2\theta\Delta & \cos 2\theta\Delta\end{pmatrix} \times \begin{pmatrix}\nu_e(t)\\ \nu_\alpha(t)\end{pmatrix}, \tag{16}$$

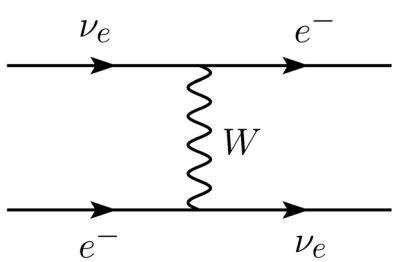

Fig. 1. Forward scattering of an electron neutrino on an electron mediated by the charged-current interaction.

This article is copyrighted as indicated in the article. Reuse of AAPT content is subject to the terms at: http://scitation.aip.org/termsconditions. Downloaded to IP: 207.207.127.233 On: Wed, 06 May 2015 16:28:56

where we emphasize the local dependence of the potential attributable to the electron number density $N_e(x)$. For relatively heavy stable nuclei, we can assume that there is roughly one electron per two nucleons in an atom, so that the electron density can be written in terms of the mass density of the matter, $N_e(x) = \rho(x)/(2m_N)$, with m_N the nucleon mass. If we express the mass density in units of g/cm^3, then this yields the potential

$$V(x) = 3.76 \times 10^{-14} \frac{\rho}{\text{g/cm}^3} \text{ eV}. \tag{17}$$

For a region of constant electron density, the solution to Eq. (16) exactly follows the vacuum case, Eq. (6); however, it is more instructive to first diagonalize H_m. If we were to diagonalize the vacuum Hamiltonian H_0, we would find that the difference in its eigenvalues would be the mass-squared difference and its eigenvectors would be the mass eigenstates. Likewise, diagonalizing H_m yields eigenvalues whose difference is the *effective* mass-squared difference Δ_m and eigenvectors that are the *effective* mass eigenstates in matter. We can make H_m traceless, since adding a multiple of the identity results in unmeasurable phase. In doing so, the matter Hamiltonian takes a simple form

$$H_\text{m} = \frac{\Delta_\text{m}}{4E} \begin{pmatrix} -\cos 2\theta_\text{m} & \sin 2\theta_\text{m} \\ \sin 2\theta_\text{m} & \cos 2\theta_\text{m} \end{pmatrix}, \tag{18}$$

with the effective mass-squared difference given by

$$\Delta_\text{m} = \Delta \sqrt{(\cos 2\theta - 2EV/\Delta)^2 + \sin^2 2\theta}, \tag{19}$$

and the effective matter mixing angle given by

$$\sin 2\theta_\text{m} = \frac{\sin 2\theta}{\sqrt{(\cos 2\theta - 2EV/\Delta)^2 + \sin^2 2\theta}}. \tag{20}$$

By analogy with the vacuum case, the oscillation probability in matter of constant density is

$$\mathcal{P}_{e\to\alpha}(L) = \sin^2 2\theta_\text{m} \sin^2\left(\frac{\Delta_\text{m} L}{4E}\right). \tag{21}$$

Referring to Eq. (20), we see that the oscillation probability can reach unity if the neutrino energy is at the MSW resonance energy, $E_R = \Delta \cos 2\theta/2V$. For neutrinos that travel through the Earth's interior, the matter density ranges from 3 g/cm^3 in the mantle to 15 g/cm^3 in the Earth's core.[18] This results in MSW resonance energies that range from 140 MeV in the mantle to 30 MeV in the core. In Fig. 2, we plot the ratio $\sin 2\theta_\text{m}/\sin 2\theta$ as a function of energy for a fixed density and vacuum mixing angle $\theta = 34°$. We also show Δ_m/Δ. Focusing on the matter mixing angle, we see that maximal mixing is achieved at the resonance and then the oscillation amplitude decreases as $1/E$ far beyond the resonance. The effective mass-squared difference exhibits the inverse behavior.

In Fig. 3, we plot the $\nu_e \to \nu_\alpha$ oscillation probability within regions of constant density; all curves employ the same energy $E = 100$ MeV and vacuum mixing angle $\theta = 34°$. Vacuum oscillations are depicted by the solid curve. Given the mixing angle, we see that the maximum probability of measuring a ν_α neutrino produced by a ν_e source is

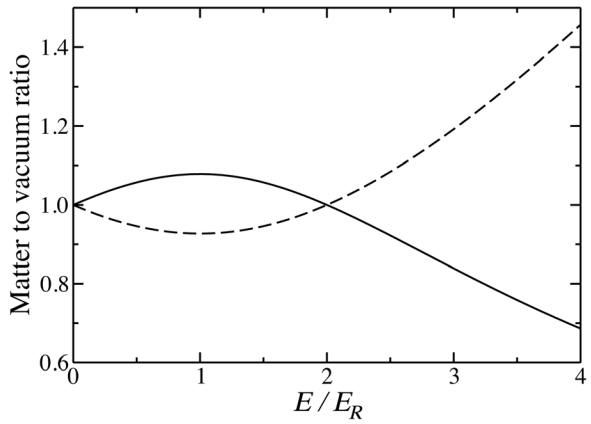

Fig. 2. The solid line is a plot of the ratio $\sin 2\theta_\text{m}/\sin 2\theta$ as a function of energy in units of the resonance energy. The dashed line is a plot of the ratio Δ_m/Δ as a function of energy. Both curves use the vacuum mixing angle $\theta = 34°$.

$\sin^2 2\theta = 0.86$. For the dotted curve, we dial up the density of matter through which the neutrinos travel so that the neutrino's energy matches the MSW resonance energy, namely $\rho = 3.75$ g/cm^3. As expected, the maximum oscillation probability rises to unity, and consistent with Fig. 2, the wavelength of oscillation in matter slightly increases. Further increasing the density, we select a value $\rho = 15$ g/cm^3 that results in $E = 4E_R$. As we are far beyond the resonance, we see that the amplitude of the oscillation is diminished by more than 50%, consistent with Fig. 2.

IV. PIECEWISE-CONSTANT DENSITY PROFILE

Using the results from the two previous sections, we can construct the oscillation probability for a neutrino traveling through matter with a piecewise-constant density profile. It is illustrative to consider one of the simplest examples of such a profile, which is relevant for neutrinos that traverse the Earth's core. We will suppose that the neutrinos travel through a region of constant density ρ_A but encounter a region of length L_B with a different constant density ρ_B. Specifically, the neutrinos see an effective potential

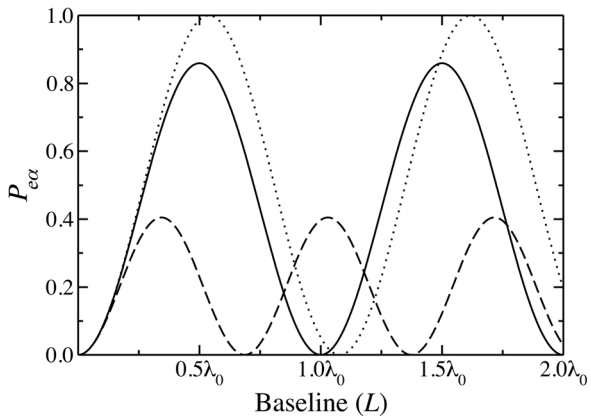

Fig. 3. Oscillation probability $\mathcal{P}_{e\to\alpha}$ in vacuum or constant-density matter with fixed vacuum mixing angle $\theta = 34°$ and energy $E = 100$ MeV. The baseline is expressed in terms of the vacuum oscillation wavelength $\lambda_0 = 3300$ km. The solid line depicts vacuum oscillations. For the dotted line, the density is $\rho = 3.75$ g/cm^3 so that $E = E_R$. For the dashed line, the density is $\rho = 15$ g/cm^3 so that $E = 4E_R$.

This article is copyrighted as indicated in the article. Reuse of AAPT content is subject to the terms at: http://scitation.aip.org/termsconditions. Downloaded to IP: 207.207.127.233 On: Wed, 06 May 2015 16:28:56

$$V(x) = \begin{cases} V_A & \text{for} \quad 0 \le x < L_A \\ V_B & \text{for} \quad L_A \le x < L_A + L_B \\ V_A & \text{for} \quad L_A + L_B \le x < L\,, \end{cases} \tag{22}$$

where the last vacuum region has length L'_A so that $L = L_A + L_B + L'_A$. If the initial neutrino state is $\nu(0)$, then we sew together the evolution operators from the constant density solutions,

$$\nu(L) = \exp[-iH_A L'_A]\exp[-iH_B L_B]\exp[-iH_A L_A]\nu(0), \tag{23}$$

where H_A and H_B refer to the matter Hamiltonian, Eq. (18), with densities ρ_A and ρ_B. Though we could write an analytical expression for the oscillation probability, it would be opaque. Instead, we will consider a few numerical solutions to showcase the dependence of the probability on both the size and placement of the inhomogeneity. So that we can continue to neglect $\Delta_{31} \simeq \Delta_{32}$ oscillations, we require $L/E \gg 1$ km/MeV. If we consider atmospheric neutrinos that travel along chords through the Earth's interior, then the baselines under consideration are on the order of 10^3 km or more. To be definite, we will consider neutrinos with energies of 200 MeV; this energy safely justifies our two-neutrino framework. Employing matter densities consistent with the Earth's interior,[18] we set $\rho_A = 5$ g/cm^3 and $\rho_B = 15$ g/cm^3. These densities correspond to oscillation wavelengths $\lambda_A = 5900$ km and $\lambda_B = 2370$ km, respectively.

In Fig. 4, we plot the oscillation probability for the piecewise-constant density profile in Eq. (22) for two different lengths L_B. In panel (a), the inhomogeneity has a length equal to an integer number of wavelengths, $4\lambda_B$. In such a situation, the oscillation probability in the subsequent region has the usual amplitude and appears only phase-shifted relative to the oscillation probability if the higher density region were not present. To contrast, in panel (b), the higher density region is positioned at the same point L_A but with a width that is an integer plus one-half wavelengths, $3.5\lambda_B$. Upon exiting this denser region, the oscillations now exhibit an enhanced probability of ν_α detection with an increased amplitude of oscillation and overall offset from zero.

This second result is somewhat surprising. From Fig. 3, we see that if the neutrino energy is greater than the MSW resonance, then the amplitude of oscillation is diminished relative to the vacuum; however, this apparently does not hold if the density of matter is not constant. In the matter of density ρ_B, the amplitude is greater than $\sin^2 2\theta_B$, and in the second vacuum region, the amplitude exceeds $\sin^2 2\theta_A$. This is counterintuitive in light of Eq. (21), but the resolution lies in the fact that, when deriving the constant density oscillation formulae, we required that the initial neutrino state have definite flavor. In Fig. 4, at the boundaries between the regions, the neutrino state is neither purely ν_e nor ν_α; instead, it is more generally $\nu = (\xi, \chi)^T$ with $|\xi|^2 + |\chi|^2 = 1$. This can modify the amplitude and offset of the oscillation probability; a specific illustration will follow. We make one final point regarding panel (a) of Fig. 4. If the matter inhomogeneity is an integer number of wavelengths (in the region), then the state of the system leaving the inhomogeneity is essentially the same as the state entering the region; as such, the inhomogeneity can produce only a phase shift in the oscillation probability.

In Fig. 5, we compare higher density regions of the same lengths but located at different positions, L_A. We set L_B to be an integer plus one-half wavelengths. In panel (a), the value for L_A is $2.5\lambda_A$. We see the oscillation probability rise to unity upon exiting the block of matter. Generally, if we were to create a periodic matter profile satisfying this half-wavelength condition for both regions, then the oscillation probability would eventually rise to unity regardless of the value of the vacuum mixing angle or the effective matter mixing angle.[31] This phenomenon is the analog of parametric resonance in mechanical systems; it was first appreciated in Ref. 32. In panel (b), the higher density region is at the position $L_A = 2\lambda_A$. Again, here the oscillation probability is diminished upon exiting the higher density region.

Let us explore in detail two particular transitions between matter regions in Fig. 5. First, in panel (a), we note that at the first transition at L_A the state of the system is $\nu = (\cos 2\theta_A, -\sin 2\theta_A)^T$, up to a phase. A similar expression

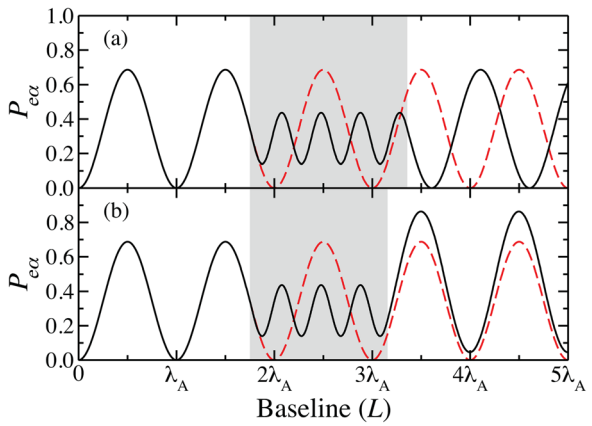

Fig. 4. The solid curves depict the oscillation probability for 200 MeV neutrinos traveling through the density profile in Eq. (22) with $\rho_A = 5$ g/cm^3 and $\rho_B = 15$ g/cm^3. The white areas indicate the regions of density ρ_A, and the shaded areas represent the regions of density ρ_B. The dashed lines represent the oscillation probability were the higher density region not present. The vacuum mixing angle is $\theta = 34°$, $\lambda_A = 5900$ km, and $\lambda_B = 2370$ km. For (a), $L_A = 1.75\lambda_A$ and $L_B = 4\lambda_B$. For (b), $L_A = 1.75\lambda_A$ and $L_B = 3.5\lambda_B$.

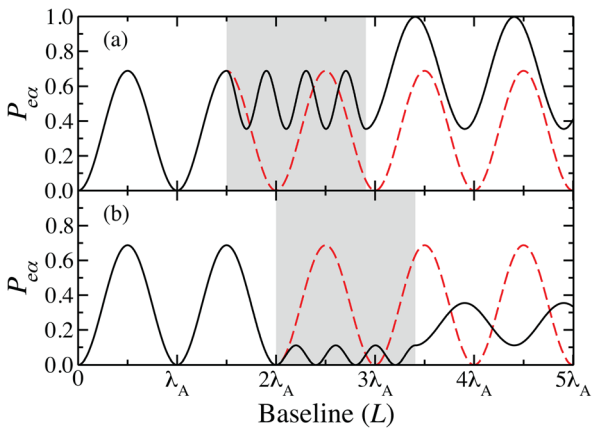

Fig. 5. The solid curves depict the oscillation probability for 200 MeV neutrinos traveling through the density profile in Eq. (22) with $\rho_A = 5$ g/cm^3 and $\rho_B = 15$ g/cm^3. The white areas indicate the regions of density ρ_A, and the shaded areas represent the regions of density ρ_B. The dashed lines represent the oscillation probability were the higher density region not present. The vacuum mixing angle is $\theta = 34°$, $\lambda_A = 5900$ km, and $\lambda_B = 2370$ km. For (a), $L_A = 1.5\lambda_A$ and $L_B = 3.5\lambda_B$. For (b), $L_A = 2\lambda_A$ and $L_B = 3.5\lambda_B$.

This article is copyrighted as indicated in the article. Reuse of AAPT content is subject to the terms at: http://scitation.aip.org/termsconditions. Downloaded to IP: 207.207.127.233 On: Wed, 06 May 2015 16:28:56

holds for the system in panel (b). At the transition located at $L_A + L_B$, the state is $\nu = (\cos 2\theta_B, -\sin 2\theta_B)^T$, up to a phase. In both cases, we will refer to the mixing angle to the left of these boundaries with the subscript 1 so that we can simply say that the state is $\nu(0) = (\cos 2\theta_1, -\sin 2\theta_1)^T$. For the region to the right of the boundary, we will denote the effective mixing angle and mass-squared difference with θ_2 and Δ_2, respectively. Then, in region 2, we have $\nu(L_2) = \exp[-iH_2L_2]\nu(0)$ as usual, leading to the oscillation probability

$$\mathcal{P}_{e\to\alpha}(L_2) = \sin 2\theta_2 \sin(2\theta_2 - 4\theta_1)\sin^2\left(\frac{\Delta_2 L_2}{4E}\right) + \sin^2 2\theta_1. \tag{24}$$

In this particular case, we see explicitly that the unexpected amplitude of oscillation and offset from zero in region 2 are results of the mixed initial state $\nu(0)$ at the boundary between the regions.

V. THE INVERSION PROBLEM: LOW DENSITY LIMIT

Neutrino tomography is the use of a neutrino beam to determine the matter profile through which the beam passes; this is essentially the inverse of the problem presented in Sec. IV. Possible applications of neutrino tomography would be to complement geophysical measurements of the profile of the Earth's interior or to find large deposits of oil.[33] A realistic study of tomography indicates that a precise determination of such profiles will be challenging, with statistics being a limitation even when the neutrino oscillation parameters become precisely known.[19]

To demonstrate the essential physics of tomography, we will consider an idealized example in which the neutrino oscillation parameters are known to high precision. We also imagine an idealized source with well-characterized spectrum and an idealized detector with sufficient resolution. We will consider the situation in which a broad spectrum beam of neutrinos travels through a region of matter that has constant density ρ_A aside from an inhomogeneity of length L_B and density ρ_B, Eq. (22). By analyzing mock neutrino "data" at the detector [computed from Eq. (23)], we hope to be able to determine L_A, L_B, and the electron density of the inhomogeneity.

A general solution to the inversion problem for the piecewise-constant density profile does not exist, but headway can be made if one has *some* information about the matter. For instance, if it is not too dense[34] (or, rather, the neutrino energy is less than the MSW resonance) and if the inhomogeneous region is not too long (relative to the oscillation wavelength in medium A), then the oscillation probability in the presence of the inhomogeneity simplifies appreciably. Formally, for the first approximation, we require $E \ll E_{R_{A,B}}$ for both regions. These conditions can be satisfied for an arbitrary energy as long as the densities are small enough. Defining $E_{\delta V} = (E_{R_B}^{-1} - E_{R_A}^{-1})^{-1}$, we expand in a Taylor series the effective mass squared difference and mixing angle in region B relative to their values in region A:

$$\Delta_B = \Delta_A\left(1 - \cos^2 2\theta\frac{E}{E_{\delta V}}\right) + \mathcal{O}\left(\frac{E^2}{E_{R_{A,B}}^2}\right), \tag{25}$$

$$\sin 2\theta_B = \sin 2\theta_A\left(1 + \cos^2 2\theta\frac{E}{E_{\delta V}}\right) + \mathcal{O}\left(\frac{E^2}{E_{R_{A,B}}^2}\right). \tag{26}$$

Additionally, we consider a relatively short inhomogeneity, that is, $L_B \ll \lambda_A$. Recalling that $\lambda_A = 4\pi E/\Delta_A$, this limit effectively places a lower bound upon the neutrino energy for a given L_B. To implement this approximation, we expand the relevant functions to first order in L_B/λ_A:

$$\sin\left(\frac{\Delta_A L_B}{4E}\right) = \frac{\Delta_A L_B}{4E} + \mathcal{O}\left(\frac{L_B^3}{\lambda_A^3}\right), \tag{27}$$

$$\cos\left(\frac{\Delta_A L_B}{4E}\right) = 1 + \mathcal{O}\left(\frac{L_B^2}{\lambda_A^2}\right). \tag{28}$$

Neglecting any terms second-order in the "small" quantities, we find that the difference between the oscillation probability with the inhomogeneity in place and the constant-density scenario takes a simple form

$$\delta\mathcal{P}_{e\to\alpha}(L) \simeq (V_B - V_A)L_B\sin^2 2\theta_A\cos 2\theta \times\left[\cos\left(\frac{\Delta_A L}{4E}\right) - \cos\left(\frac{\Delta_A(2L_A - L)}{4E}\right)\right]\sin\left(\frac{\Delta_A L}{4E}\right). \tag{29}$$

Since the distance L is fixed and the energy is actually varied in our thought experiment, we prefer to think of this quantity in terms of $\omega = \Delta_A/4E$. Then, a Fourier transform of $\delta\mathcal{P}_{e\to\alpha}(\omega)$ allows one to determine L_A:

$$\begin{aligned}\widehat{\delta\mathcal{P}_{e\to\alpha}}(\ell) &= \frac{1}{\sqrt{2\pi}}\int_{-\infty}^{\infty}\delta\mathcal{P}_{e\to\alpha}(\omega)e^{-i\omega\ell}\,d\omega \\ &\simeq \frac{i\sqrt{\pi}(V_B - V_A)L_B\sin^2 2\theta_A\cos 2\theta}{2\sqrt{2}} \\ &\quad\times[\delta(\ell - 2L) - \delta(\ell + 2L) + \delta(\ell + 2L_A) \\ &\quad - \delta(\ell - 2L_A) + \delta(\ell + 2L - 2L_A) \\ &\quad -\delta(\ell - 2L + 2L_A)],\end{aligned} \tag{30}$$

where we use expression (29) to approximate the transform.

The experimental procedure is now clear. If the spectrum of the neutrino beam is chosen to satisfy the two requirements $\Delta_A L_B \ll E \ll E_R$, one can compare the measured neutrinos at the detector to the constant-density oscillation expectations; that is, one can measure $\delta\mathcal{P}_{e\to\alpha}(\omega)$. A Fourier transform of these data can allow one to determine L_A, and then from the amplitude of $\delta\mathcal{P}_{e\to\alpha}(\omega)$, one can determine the product $(V_B - V_A)L_B$, making use of L_A in Eq. (29). At this level of approximation, one cannot independently determine V_B or L_B. On the theoretical side, this can be rectified by including higher-order terms in the Taylor expansion involving L_B; however, on the experimental front, the data would need to have a higher energy resolution. Regardless, at the present level of approximation, if one happens to know the electron density of the inhomogeneity (say, it is a particular type of ore or a petroleum deposit), then L_B can be determined.

To be explicit, we assume our source to be reactor anti-neutrinos traveling through the Earth's mantle, and we set $\rho_A = 3.0$ g/cm^3. The spectrum of electron anti-neutrinos

This article is copyrighted as indicated in the article. Reuse of AAPT content is subject to the terms at: http://scitation.aip.org/termsconditions. Downloaded to IP: 207.207.127.233 On: Wed, 06 May 2015 16:28:56

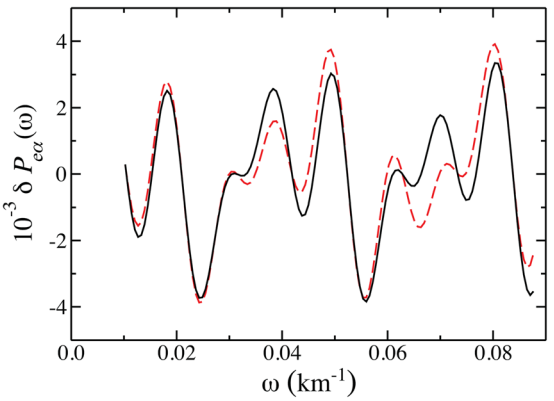

Fig. 6. The difference in oscillation probabilities, $\delta\mathcal{P}_{e\to\alpha}(\omega)$, for $L_A = 90$ km, $L_B = 10$ km, and $L = 300$ km. The vacuum mixing angle is $\theta = 34^\circ$, and the matter densities are $\rho_A = 3$ g/cm^3 and $\rho_B = 8$ g/cm^3. The anti-neutrino energy ranges from 1 to 10 MeV. The solid curve is computed without approximation from Eq. (23). The dashed curve is computed from the approximate expression in Eq. (29).

from a reactor is well known,[35] but for simplicity we will take the spectrum to be flat from 1 MeV to 10 MeV with a detector energy resolution that ranges from 0.5% to 5%. This range of energies is well below the resonant energy for Δ_{21} oscillations even for core densities that approach 15 g/cm^3. We fix the source-to-detector baseline to be 300 km. From the low to the high end of the spectrum, the oscillation wavelength in the mantle ranges from 30 to 300 km, restricting the size of the inhomogeneity to be on the order of tens of kilometers. We choose the size of the inhomogeneity be $L_B = 10$ km with a density of 8 g/cm^3, located at a position $L_A = 90$ km. Using the exact evolution, Eq. (23), we can generate mock idealized data cast in terms of the function $\delta\mathcal{P}_{e\to\alpha}(\omega)$. In Fig. 6, the solid curve represents these data over the relevant energy range. In the same figure, the dashed curve represents a calculation of $\delta\mathcal{P}_{e\to\alpha}(\omega)$ using the approximate expression in Eq. (29), valid for low-density, small inhomogeneities. The two curves agree rather well for lower values of ω (i.e., higher values of the energy). As ω increases (the energy decreases), the approximation worsens as the errors incurred from the finite size of the inhomogeneity become significant.

With these data, we use the FFT routine in Grace,[36] a graphical program, to compute the magnitude of the Fourier transform of $\delta\mathcal{P}_{e\to\alpha}(\omega)$, displayed in Fig. 7. We identify

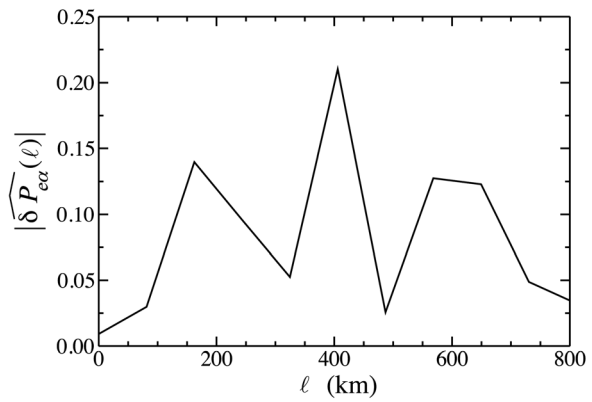

Fig. 7. The magnitude of the Fourier transform of $\delta\mathcal{P}_{e\to\alpha}(\omega)$. Only positive values of ℓ are shown.

three peaks corresponding to $\ell = 2L_A$, $2(L - L_A)$, and $2L$, per Eq. (30). The peak with the largest value of ℓ is located at approximately 609 km and corresponds to $2L$, implying $L \simeq 305$ km. This is consistent with the experimental setup, given the limited resolution of the mock data. There is ambiguity in the identity of the two remaining peaks. It could be that the $\ell = 406$ km peak corresponds to $2L_A$, or it is possible that the other peak at $\ell = 162$ km corresponds to $2L_A$. If we were to compute the Fourier transform of the *exact* expression for $\delta\mathcal{P}_{e\to\alpha}(\omega)$, we would find that this degeneracy, though somewhat modified, would remain; in particular, the oscillation probability at the detector, $\mathcal{P}_{e\to\alpha}(L)$, is invariant under the interchange $L_A \leftrightarrow L'_A$. This speaks to the presence of a symmetry in the system. Generally, if the mixing matrix U is real,[37] then the system is invariant under time reversal. That is to say, if the state ν_α travels from the source through the matter profile and is detected as state ν_β at the detector, then with equal probability we expect the state ν_β, starting at the detector and traveling the *opposite* direction through the matter, to be detected as the state ν_α at the source. Symbolically, we write this as $\mathcal{P}_{\alpha\to\beta}(L) = \mathcal{P}_{\beta\to\alpha}(-L)$, where the negative sign in the second argument indicates a reversal of the orientation of the neutrino's path. Applying time reversal to the present situation implies $\mathcal{P}_{e\to\alpha}(L) = \mathcal{P}_{\alpha\to e}(-L)$; however, this does not explain the above degeneracy. What we need to show is $\mathcal{P}_{e\to\alpha}(L) = \mathcal{P}_{e\to\alpha}(-L)$. For a three-neutrino system, this statement is *not* true, but for a two-state system, it happens to be true. Generically, if the initial and final states are the same, then we have $\mathcal{P}_{e\to e}(L) = \mathcal{P}_{e\to e}(-L)$. But, in our two-state system, the sum of the appearance and survival probabilities is unity, so that $\mathcal{P}_{e\to e}(L) = 1 - \mathcal{P}_{e\to\alpha}(L)$; this yields the desired result.

In short, we can determine the position of the inhomogeneity only up to a two-fold degeneracy; in this case, either $L_A \simeq 203$ km or $L_A \simeq 81$ km. With knowledge of L_A, we can then fit the data to the approximate form for $\delta\mathcal{P}_{e\to\alpha}(\omega_0)$, Eq. (29), to determine $(V_B - V_A)L_B$. These results are predicated upon the assumption that one could actually realize the necessary energy resolution and be sensitive to deviations in the oscillation probability at the level of less than a percent. The energy resolution is not unreasonable, as it compares favorably to another reactor anti-neutrino detector.[8] As for the measurements of the oscillation probability, both statistical and systematic errors would currently limit the ability to push the measurements down to the needed level of precision for the scenario presented. If the size of the inhomogeneous region were larger, then the oscillation probability could differ from the constant-density oscillation probability at a measurable level. One could then extract information about the inhomogeneity from $\delta\mathcal{P}_{e\to\alpha}(\omega)$, but the analysis would more than likely require Monte Carlo simulations rather than a mere Fourier transform.

VI. CONCLUDING REMARKS

For a two-neutrino system, we developed the evolution equation for propagation in vacuum and in constant-density matter, allowing us to calculate the oscillation probability for these cases. Using these results, we are able to compute the oscillation probability for neutrinos that travel through a region with a piecewise-constant density profile. Focusing upon a simple profile, we show how both the size and position of an inhomogeneity have nontrivial consequences for the oscillation probability. The enhancement of the probability for

This article is copyrighted as indicated in the article. Reuse of AAPT content is subject to the terms at: http://scitation.aip.org/termsconditions. Downloaded to IP: 207.207.127.233 On: Wed, 06 May 2015 16:28:56

the situation depicted in Fig. 5(a) has important implications for modeling atmospheric neutrinos that pass through the interior of the Earth, whose density is approximately piecewise-constant. Inverting the problem, we show how an idealized beam of neutrinos can be used to assess the density profile of the medium through which they travel. Considering a simple profile in the low-density and small-size inhomogeneity limits, we show that by comparing the measured oscillation probability to its constant-density value one can determine (up to a twofold degeneracy) the position of the inhomogeneity and the product of its density and length.

Several extensions of these calculations naturally arise. One could explore neutrino tomography with the same simple model considered above but instead examine different energy regimes. In particular, one could develop approximate formulae for $\delta P_{e\to\alpha}$ for energies either near or far beyond the MSW resonance. Additionally, one can deal with more complicated density profiles. This would allow one to effect adiabatic transitions where neutrinos travel through a medium with a small density gradient; such transitions are a key component to explaining the solar neutrino problem. In short, neutrino oscillations in matter represent physically relevant but accessible two-state systems that can be studied in an introductory quantum mechanics course.

ACKNOWLEDGMENTS

The authors are grateful for useful comments from Greg Elliott, Joel Franklin, Mary James, and Jerry Shurman.

APPENDIX: THE GENERALIZED INDEX OF REFRACTION

We derive Fermi's generalized index of refraction formula.[17] This derivation is similar to that in classical electrodynamics, which results in the index of refraction for light traveling through a dilute medium.[26] We consider a plane wave $\psi(z) = Ae^{ikz}$, with wavenumber $\vec{k}_0 = k\hat{z}$, incident upon a thin uniform slab with thickness d but laterally infinite in extent; see Fig. 8. The slab needs to be thin enough so that multiple scatterings can be neglected, and we assume that the scattering centers in the slab are randomly distributed. The goal is to compute the wave function "far" from the slab at the point z_0 on the z-axis; formally, we require $kz_0 \gg 1$.

For a scattering center located at the origin of the coordinate system, the wave function consists of the original plane wave and outgoing spherical wave, assuming large r:

$$\psi(\vec{r}) = A\left(e^{ikz} + f(\theta)\frac{e^{ikr}}{r}\right). \tag{A1}$$

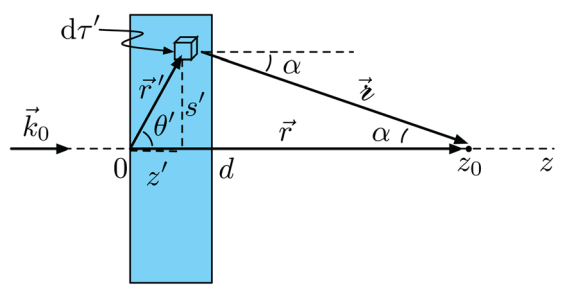

Fig. 8. A plane wave impinges upon a slab of thickness d at normal incidence. The primed coordinates refer to positions within the slab.

We assume azimuthal symmetry so that the scattering amplitude $f(\theta)$ is a function of θ only. If we displace the scattering center from the origin to a point located at $\vec{r}'$, then we must modify the scattered portion of the wave function. Supposing there are N scatterers per unit volume (assumed to be constant in the slab), then the wave function with the displaced scattering center is

$$\psi(\vec{r}) = A\left(e^{ikz} + e^{i\vec{k}_0\cdot\vec{r}'}f(\alpha)\frac{e^{ik\mathfrak{r}}}{\mathfrak{r}}Nd\tau'\right), \tag{A2}$$

where $\vec{\mathfrak{r}} = \vec{r} - \vec{r}'$ and $\cos\alpha = \hat{\mathfrak{r}}\cdot\hat{z}$. We set $\vec{r} = z_0\hat{z}$ and use cylindrical coordinates to refer to the slab. This yields the volume element $d\tau' = 2\pi s'ds'dz'$ and $\mathfrak{r}^2 = s'^2 + (z_0 - z')^2$. Integrating over the slab, the scattered portion of the wave function is

$$\psi_{\text{scatt}}(z_0\hat{z}) = A2\pi N\int_0^d dz'e^{ikz'}\int_0^\infty f(\alpha)\frac{e^{ik\mathfrak{r}}}{\mathfrak{r}}s'ds'. \tag{A3}$$

For the first integral, we can substitute variables of integration as $s'ds' = \mathfrak{r}\,d\mathfrak{r}$, changing the lower limit of integration to $|z_0 - z'|$. Using integration by parts, this integral becomes

$$\int_{|z_0-z'|}^\infty f(\alpha)e^{ik\mathfrak{r}}\,d\mathfrak{r} = \left[\frac{f(\alpha)}{ik}e^{ik\mathfrak{r}}\right]_{|z_0-z'|}^\infty - \int_{|z_0-z'|}^\infty \frac{e^{ik\mathfrak{r}}}{ik}\frac{df(\alpha)}{d\cos\alpha}\frac{d\cos\alpha}{d\mathfrak{r}}d\mathfrak{r}. \tag{A4}$$

In the integral on the right-hand side, the second derivative evaluates as $d\cos\alpha/d\mathfrak{r} = -|z_0 - z'|/\mathfrak{r}^2$; assuming that the scattering amplitude is well-behaved, this integral is suppressed by a factor of $(k\mathfrak{r})^{-1} \ll 1$ and can safely be neglected. For the surface term in Eq. (A4), the expression does not converge at the upper limit; however, since the slab is not truly laterally infinite, one typically introduces a factor that forces the density of scatterers to go to zero for large s'. We note that $\mathfrak{r} = |z_0 - z'|$ whenever $\alpha = 0$, resulting in

$$\int_{|z_0-z'|}^\infty f(\alpha)e^{ik\mathfrak{r}}\,d\mathfrak{r} \approx i\frac{f(0)}{k}e^{ik|z_0-z'|}. \tag{A5}$$

Since $z_0 > z'$, when we plug this result into the remaining integral in Eq. (A3), we find that the integrand is constant, yielding the final result

$$\psi_{\text{scatt}}(z_0\hat{z}) \approx A2\pi iNdf(0)\frac{e^{ikz_0}}{k}. \tag{A6}$$

This scattered wave, Eq. (A6), is to be compared with a plane wave that passes through a thin slab with index of refraction n and thickness d. In a material, the wavenumber becomes $\tilde{k} = nk$ so that at z_0 the wave is

$$\psi(z_0) = Ae^{ik(z_0-d)}e^{i\tilde{k}d} \approx Ae^{ikz_0}[1 + ikd(n-1)], \tag{A7}$$

given $kd \ll 1$. The index of refraction for a dilute medium is thus related to the forward scattering amplitude according to

$$n = 1 + 2\pi N\frac{f(0)}{k^2}. \tag{A8}$$

This article is copyrighted as indicated in the article. Reuse of AAPT content is subject to the terms at: http://scitation.aip.org/termsconditions. Downloaded to IP: 207.207.127.233 On: Wed, 06 May 2015 16:28:56

[1]J. N. Bahcall, M. H. Pinsonneault, and S. Basu, "Solar models: Current epoch and time dependences, neutrinos, and helioseismological properties," Astrophys. J. **555**, 990–1012 (2001).
[2]B. T. Cleveland, T. Daily, R. Davis, Jr., J. R. Distel, K. Lande, C. K. Lee, P. S. Wildenhain, and J. Ullman, "Measurement of the solar electron neutrino flux with the Homestake chlorine detector," Astrophys. J. **496**, 505–526 (1998).
[3]J. N. Abdurashitov *et al*. (SAGE Collaboration), "Solar neutrino flux measurements by the Soviet-American Gallium Experiment (SAGE) for half the 22 year solar cycle," J. Exp. Theor. Phys. **95**, 181–193 (2002).
[4]W. Hampel *et al*. (GALLEX Collaboration), "GALLEX solar neutrino observations: Results for GALLEX IV," Phys. Lett. B **447**, 127–133 (1999).
[5]Y. Fukuda *et al*. (Kamiokande Collaboration), "Solar neutrino data covering solar cycle 22," Phys. Rev. Lett. **77**, 1683–1686 (1996).
[6]B. Aharmim *et al*. (SNO Collaboration), "An Independent Measurement of the Total Active B-8 Solar Neutrino Flux Using an Array of He-3 Proportional Counters at the Sudbury Neutrino Observatory," Phys. Rev. Lett. **101**, 111301 (2008).
[7]Y. Ashie *et al*. (Super-Kamiokande Collaboration), "Evidence for an oscillatory signature in atmospheric neutrino oscillation," Phys. Rev. Lett. **93**, 101801 (2004).
[8]S. Abe *et al*. (KamLAND Collaboration), "Precision Measurement of Neutrino Oscillation Parameters with KamLAND," Phys. Rev. Lett. **100**, 221803 (2008).
[9]F. P. An *et al*. (DAYA-BAY Collaboration), "Observation of electron-antineutrino disappearance at Daya Bay," Phys. Rev. Lett. **108**, 171803 (2012).
[10]P. Adamson *et al*. (MINOS Collaboration), "Measurement of Neutrino Oscillations with the MINOS Detectors in the NuMI Beam," Phys. Rev. Lett. **101**, 131802 (2008).
[11]E. Aliu *et al*. (K2K Collaboration), "Evidence for muon neutrino oscillation in an accelerator-based experiment," Phys. Rev. Lett. **94**, 081802 (2005).
[12]M. C. Gonzalez-Garcia, M. Maltoni, and J. Salvado, "Updated global fit to three neutrino mixing: Status of the hints of $\theta_{13} > 0$," JHEP **1004**, 056 (2010).
[13]W. C. Haxton and B. R. Holstein, "Neutrino physics," Am. J. Phys. **68**, 15–32 (2000).
[14]C. Waltham, "Neutrino oscillations for dummies," Am. J. Phys. **72**, 742–752 (2004).
[15]W. C. Haxton and B. R. Holstein, "Neutrino physics: An Update," Am. J. Phys. **72**, 18–24 (2004).
[16]D. J. Griffiths, *Introduction to Quantum Mechanics*, 2nd ed. (Pearson Prentice-Hall, Upper Saddle River, NJ, 2005).
[17]E. Fermi, *Nuclear Physics*, revised ed. (University of Chicago Press, Chicago, 1950), pp. 201–202.
[18]A. M. Dziewonski and D. L. Anderson, "Preliminary reference earth model," Phys. Earth Planet. Interiors **25**, 297–356 (1981).
[19]W. Winter, "Neutrino tomography: Learning about the earth's interior using the propagation of neutrinos," Earth Moon Planets **99**, 285–307 (2006).
[20]E. K. Akhmedov, M. A. Tortola, and J. W. F. Valle, "Geotomography with solar and supernova neutrinos," JHEP **0506**, 053 (2005).
[21]B. Pontecorvo, "Neutrino experiments and the problem of conservation of leptonic charge," Sov. Phys. JETP **26**, 984–988 (1968).
[22]Z. Maki, M. Nakagawa, and S. Sakata, "Remarks on the unified model of elementary particles," Prog. Theor. Phys. **28**, 870–880 (1962).
[23]G. L. Fogli, E. Lisi, A. Marrone, D. Montanino, A. Palazzo, and A. M. Rotunno, "Global analysis of neutrino masses, mixings and phases: Entering the era of leptonic CP violation searches," Phys. Rev. D **86**, 013012 (2012).
[24]A. Goobar, S. Hannestad, E. Mortsell, and H. Tu, "A new bound on the neutrino mass from the SDSS baryon acoustic peak," JCAP **0606**, 019 (2006).
[25]R. P. Feynman, R. B. Leighton, and M. Sands, *The Feynman Lectures on Physics* (Addison-Wesley, Boston, 1963), Vol. 1, pp. 31.1–31.11.
[26]J. D. Jackson, *Classical Electrodynamics*, 3rd ed. (Wiley, New York, 1999), pp. 500–505.
[27]J. Liu, "Neutrino coherent forward scattering and its index of refraction," Phys. Rev. D **45**, 1428–1431 (1992).
[28]S. P. Mikheev and A. Y. Smirnov, "Resonance amplification of oscillations in matter and spectroscopy of solar neutrinos," Sov. J. Nucl. Phys. **42**, 913–917 (1985).
[29]L. Wolfenstein, "Neutrino oscillations in matter," Phys. Rev. D **17**, 2369–2374 (1978).
[30]D. J. Griffiths, *Introduction to Elementary Particles*, 2nd ed. (Wiley-VCH, Weinheim, 2008), pp. 307–337.
[31]E. K. Akhmedov, "Neutrino oscillations in inhomogeneous matter" (in Russian), Sov. J. Nucl. Phys. **47**, 301–302 (1988).
[32]V. K. Ermilova, V. A. Tsarev, and V. A. Chechin, "Buildup of neutrino oscillations in the earth," JETP Lett. **43**, 453–456 (1986).
[33]T. Ohlsson and W. Winter, "Could one find petroleum using neutrino oscillations in matter?," Europhys. Lett. **60**, 34–39 (2002).
[34]A. N. Ioannisian and A. Y. Smirnov, "Neutrino oscillations in low density medium," Phys. Rev. Lett. **93**, 241801 (2004).
[35]T. A. Mueller *et al*., "Improved predictions of reactor antineutrino spectra," Phys. Rev. C **83**, 054615 (2011).
[36]Grace is a two-dimensional plotting tool available at <http://plasma-gate.weizmann.ac.il/Grace/>.
[37]For a purely two-neutrino system, the mixing matrix can always be taken as real since complex phases can be absorbed into the definitions of the fields. For a three-neutrino system, this is not the case. Three complex phases survive, though only one of these, the Dirac CP phase, is observable in neutrino oscillations.

MAKE YOUR ONLINE MANUSCRIPTS COME ALIVE

If a picture is worth a thousand words, videos or animation may be worth a million. If you submit a manuscript that includes an experiment or computer simulation, why not make a video clip of the experiment or an animation of the simulation. These files can be placed on the Supplementary Material server with a direct link from your manuscript. In addition, video files can be directly linked to the online version of your article, giving readers instant access to your movies and adding significant value to your article.

See http://ajp.dickinson.edu/Contributors/EPAPS.html for more information.

This article is copyrighted as indicated in the article. Reuse of AAPT content is subject to the terms at: http://scitation.aip.org/termsconditions. Downloaded to IP: 207.207.127.233 On: Wed, 06 May 2015 16:28:56